RESEARCH ARTICLE

Removal of crystal violet dye using grafted guar gum along with nanoclay and MWCNT

Fiza Simran[1], Prathiksha Karumbaiah[1], Pratik Roy[2,], R.R.N. Sailaja[2]*

The present study is aimed to remove toxic crystal violet dye from aqueous solutions. In this study guar gum (GG) has been grafted with acrylic acid (AA) by following microwave assisted grafting method. Two different nanomaterials i.e., nanoclay (NC) and multiwalled carbon nanotubes (MWCNT) has been incorporated either alone or in combination during the grafting reaction. The synthesized nanocomposites have been used for removal of crystal violet dye from aqueous solutions. Study showed higher dye adsorption capacity of the synthesized composites after addition of nanomaterials. The adsorption isotherm followed both Langmuir and Freundlich model. It was found that GG grafted AA composite with MWCNT showed highest crystal violet dye adsorption compared to others. Swelling behaviour of the synthesized composites in acidic, neutral and alkaline medium has been studied. The swelling kinetics in acidic, neutral and alkaline medium was found to follow pseudo second order kinetic model with $<R^2>$ value more than 0.98. Fourier transform infrared spectroscopy (FTIR) showed efficient grafting of AA on GG. X-ray diffraction (XRD) and morphological characteristics depicted enhanced dispersion of nanomaterials in GG matrix.

The contamination of water bodies increased with increase in industrial development. Hence it has become essential to remove these toxic contaminants by eco-friendly means. Polysaccharide such as guar gum is inexpensive and can be used for such applications [**1**]. Hence guar gum has a promising potential to be an adsorbent for removal of dyes. The removal of acid dyes using plant based gums has been reviewed by Verma *et.al.*, [**2**]. It was found that gum based materials are highly efficient in dye removal from textile waste waters. A review of polysaccharide grafted co-polymeric hydrogels suggested that guar gum due to its non-ionic nature can be modified to suit the targeted contaminant [**3**]. Thermodynamic studies on guar gum/bentonite nanocomposites for removal of heavy metal and dye revealed endothermic spontaneous process at solid-solution interface [**4**]. Duan et.al used hydrazine modified guar gum for removal of various dyes. The dye adsorption was found to follow Langmuir model [**5**]. Vanaamudan *et.al.*, [**6**] studied chitosan- guar gum blend loaded with silver nanoparticles and used it for catalytic degradation of dyes. The catalyst could be used up to three cycles. Patra et.al used modified guar-gum loaded with silica nanoparticles for selective removal of methylene blue and congo red dyes. The developed nanocomposites showed better adsorption capacity than neat guar gum [**7**]. Modified guar gum with iron and soya lecithin was used for the removal of methyl violet dye by Sharma et.al. The developed hydrogel showed high adsorption capacity along with efficient photocatalytic activity [**8**]. Hydrogels using modified guar gum showed both antibacterial properties and dye adsorption capacity for methylene blue. Hence, modified guar gum could overcome the limitation of instability and microbial contamination [**9**]. Iron-oxide nanoparticles coated with guar gum showed effective removal of congo red dye and adsorption was found to follow Langmuir isotherm as observed by Sahoo et.al [**10**]. Acrylic acid modified xanthan gum along with reduced graphene oxide could efficiently adsorb methylene blue dye by following pseudo-second order kinetic and Langmuir adsorption isotherm respectively [**11**]. Similar modification of guar gum by borax crosslinking and manganese dioxide showed high efficiency in methylene blue removal along with good recyclability [**12**]. Adsorption of guar gum powder for removal methyl red showed adsorbability which follows Langmuir isotherm model [**13**]. Pakdel *et.al.*, reviewed the applications of acrylic based hydrogels. It was envisaged that acrylics can form complexes with metal cations and certain dyes. Hence it has a promising potential for removal of both heavy metals and dyes from waste water [**14**]. Our earlier work on guar gum grafted acrylic acid with nanoclay gave encouraging results [**15**] for removal of crystal violet dye. In that study the emphasis was mainly on microwave assisted synthesis and optimization

[1]The Oxford College of Engineering, Bangalore 560068, India
[2]The Energy and Resources Institute, Southern Regional Centre, Bangalore 560071, India

*Corresponding author:
E-mail: protiik.roy@gmail.com

DOI: 10.5185/amlett.2022.011686

of reaction parameters. In this study we have made further studies on adsorbent dosage and analysis using isotherm models. Further, guar gum grafted acrylic acid along with MWCNT has also been prepared in-situ. The removal of crystal violet dye has been analyzed and the performance of both the modified guar gum nanocomposites has been compared.

Materials and methods

Materials

Guar gum (GG) used in this study was purchased from S.d. Fine Chem, Mumbai (India). Acrylic acid (AA) was procured from N.R. CHEM, Mumbai (India). Nanoclay (NC) (Montmorillonite clay surface modified with 15-35 wt% octadecylamine and 0.5-5 wt% aminopropyl triethoxy silane) was purchased from Sigma Aldrich, USA. Acid modified multiwalled carbon nanotubes (MWCNT) were procured from Global Nanotech, Mumbai (India). Ammonium persulfate and N.N-methylbisacrylamide was obtained from S.d. Fine Chem, Mumbai, India. Crystal violet dye was purchased from Himedia Laboratories, Mumbai (India). All other solvents used were obtained from S.d. Fine Chemicals, Bangalore (India) and were used as received.

Synthesis of Guar gum-g-acrylic acid (GG-g-AA)

3g of guar gum was dissolved in 400 ml of distilled water and 18 ml of acrylic acid was added to the guar gum solution and stirred for 20 minutes. 0.27 g of ammonium persulphate (APS) initiator and 0.27 g of N, N-methylene bisacrylamide (MBA) cross linker was added to the mixture and stirred for 90 minutes at 60℃.The reaction mixture of acrylic acid grafted guar gum was cooled to room temperature. In order to remove unreacted acrylic acid and homopolymer, the mixture was neutralized using 1N NaOH solution till the pH reaches 7. This was followed by precipitation using acetone. The precipitate obtained was washed several times with acetone and kept for drying at 70˚C for 6-12 hours.

For the synthesis of GG-g-AA with nanoclay (NC), and acid modified MWCNT (separately), similar procedure was followed except that the nanoparticles (0.5%) were added to the GG and AA mixture and sonicated for about 30 minutes using Ultra Sonicator (Branson, 2510E/DTH) prior to the reaction.

Fourier transform infrared (FTIR) spectroscopy

The Fourier transform infrared spectroscopy (FTIR) spectra of pure guar gum and GG-g-AA were carried out by using FTIR Spectrophotometer (Bruker ALPHA FT-IR Spectrometer) between 600 and 4000 cm^{-1}.

X-ray diffraction (XRD) studies

X-ray diffraction (XRD) measurements for the composites have been performed using advanced diffractometer (PAN alytical, XPERT-PRO) equipped with Cu-Kα radiation source (X = 0.154 nm). The diffraction data were collected in the range of 2θ = 2–60° using a fixed time mode with a step interval of 0.05°.

Scanning electron microscopy (SEM)

The morphological characterization of the specimen were carried out using a Scanning Electron Microscope (SEM) (HITACHI TM4000 Tabletop Microscope). The specimens were gold sputtered prior to microscopy.

Transmission electron microscopy (TEM)

Transmission electron microscopy (TEM) for nanocomposites has been performed using a JEOL, Model 782, operating at 200 kV. TEM specimens were prepared by dispersing the composite powders in methanol by ultrasonication. A drop of the suspension was put on a TEM support grid (300 mesh copper grid coated with carbon). After drying in air, the composite powder remained attached to the grid and was viewed under the transmission electron microscope.

Water absorbency and swelling kinetics

Swelling studies of the absorbent materials namely guar gum grafted acrylic acid (GG-g-AA), guar gum grafted acrylic acid with nanoclay (GG-g-AA/NC) and guar gum grafted acrylic acid with multi-walled carbon nanotubes (GG-g-AA/MWCNT) at various buffer mediums were measured as follows: 0.1 ± 0.02 g of samples were placed in 25 ml beakers into which 10 ml of buffer solutions with pH 7, pH 9 and pH 4 were then added separately. The weight of swollen sample was noted every 10 minutes till it reached equilibrium. The excess water on the surface was removed by gently tapping the swollen sample with a dry filter paper. Swelling (S) of sample was measured by weighing the swollen and the dry samples. Swelling (S) of sample was calculated using the equation given below.

$$\text{Swelling (S) in (g/g)} = \frac{(W_t - W_0)}{W_0} \quad (1)$$

where, W_0 and W_t are the weights of the dry sample and the swollen sample at the time t, respectively.
The equilibrium swelling (E_S) of sample was calculated by using following equation:

$$\text{Equilibrium Swelling } (E_S) \text{ in (g/g)} = \frac{(W_e - W_0)}{W_0} \quad (2)$$

Here W_e is the mass of the swollen sample at equilibrium.

Dye removal studies

Dye adsorption for guar gum grafted acrylic acid (GG-g-AA) with 0.5% nanoclay (NC), 0.5% MWCNT, 0.5% NC + 0.5% MWCNT and control was carried out by immersing 0.1, 0.15 and 0.2g of adsorbent respectively for each composite in 10ml of dye solution separately. Adsorption kinetics study was examined through batch method at specified time intervals using different concentration of methyl violet dye. All adsorption experiments were assessed using UV spectrophotometer at

λ_{max}= 590nm. The dye removal percentage (R%) and the adsorption capacity or dye removal efficiency (q_t, mg/g) was calculated using following Equations given below. Standard dye solution of methyl violet was prepared for three different concentrations namely 10, 30, and 50 mg/l.

$$\text{Adsorption capacity, } qt = \frac{(Co-Ct)}{m} \times V \quad (3)$$

$$\text{Dye removal percentage, } R\% = \frac{(C_o-C_e)}{C_0} \times 100 \quad (4)$$

where, C_0 is the initial dye concentration (mg/L), C_t is the remaining dye concentrations in the solution at time t (mg/L), C_e is the remaining dye concentration in the solution at equilibrium (mg/L), V is the volume of dye solution used in litres (L) and m is the weight of absorbent (mg).

Adsorption Isotherm models

Different isotherm models were applied in order to analyse the characteristics parameters of the adsorption process like adsorption capacity and adsorbate concentration. In this study, two isotherms namely Langmuir and Freundlich were used to fit the experimental data.

Langmuir model assumes formation of monolayer adsorption on a homogenous adsorbent surface and no further adsorption occurs thereafter [23]. Langmuir isotherm can be represented as liner equation as follows:

$$\frac{1}{q_e} = \frac{1}{q_m} + \frac{1}{qm*KL*Ce} \quad (5)$$

where q_m is the maximum monolayer adsorption capacity (mg/g), K_L = Langmuir isotherm constant (L/mg), C_e = equilibrium concentration of adsorbate (mg/L) and q_e = amount of adsorbate per gram of adsorbent at equilibrium (mg/g). q_m and K_L values can be obtained from slope and intercept of linear plot of $1/q_e$ versus $1/C_e$.

Freundlich isotherm model is commonly used to describe adsorption characteristics for heterogenous surface [24]. This isotherm model can be represented as follows:

$$lnq_e = \frac{1}{n_F} lnC_e + lnK_F \quad (6)$$

where K_F = Freundlich isotherm constant ($mg^{1-1/n}L^{1/n}g^{-1}$), $1/n_F$ = constant indicating adsorption intensity, C_e = equilibrium concentration of adsorbate (mg/L) and q_e = amount of adsorbate per gram of adsorbent at equilibrium (mg/g). The intercept K_F and the slope $1/n_F$ are be obtained by plotting lnq_e against lnC_e.

Results and discussion

FTIR analysis

FTIR spectrograms of pure guar gum and guar gum grafted acrylic acid are shown in **Fig. 1**. Pure guar gum shows characteristic peaks at 3430 and 2940 cm^{-1} represents characteristic –O-H stretching and –C-H stretching vibrations respectively while the peak at 1655 cm^{-1} is due to the characteristic amide I carbonyl stretching [**16**]. The peaks at 1434 and 1084 cm^{-1} depicts –C-H and –O-H bending vibrations [**15**]. Guar gum grafted acrylic acid shows a newer characteristic peak at 1737 cm^{-1} due to carbonyl stretching of the carboxylic acid which ensures the grafting reaction [**16**].

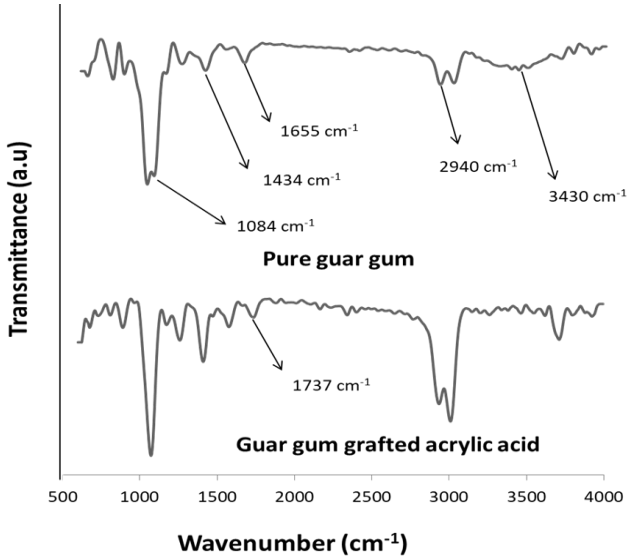

Fig 1. FTIR spectra of guar gum and guar gum grafted acrylic acid.

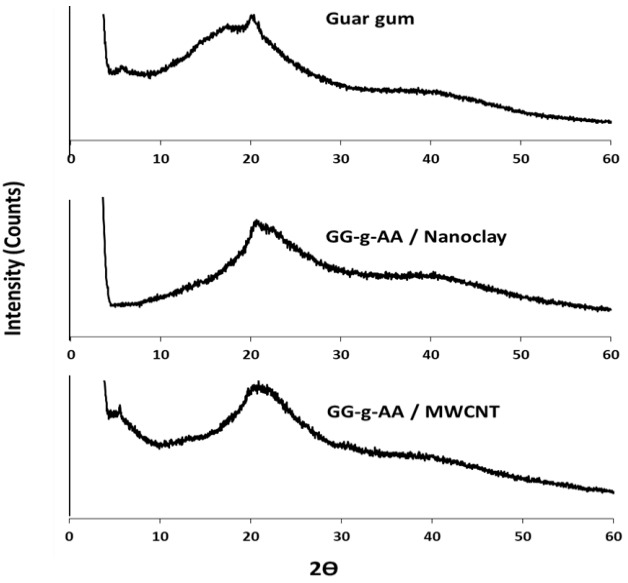

Fig. 2. X-ray diffractograms of guar gum, guar gum grafted acrylic acid with nanoclay and guar gum grafted acrylic acid with MWCNT.

XRD analysis

Fig. 2 show the XRD diffractograms for guar gum and the nanocomposites. Neat guargum has a broad amorphous peak at 2Θ value of 20.4° and very small broad peak at 40.8°. Nanoclay has sharp prominent peaks at 2Θ values

of 8.03°, 24.65°, 26.62°, 34.87° and 54.83° indicating organized clay platelets. Neat MWCNT has a main sharp narrow peak at 2Θ values of 25.7° and short broad peak at 42.55° which are attributed to an interplanar space of 3.41°A and 2.05°A respectively [**17**]. For the guargum/nanoclay composites, the peaks of nanoclay disappear suggesting that it has exfoliated. This is mainly attributed to the in-situ grafting of guar gum with acrylic acid along with nanoclay and sonication. A similar observation was made in our earlier work [**15**] and Yoonessi *et.al.,* [**18**]. A similar trend is observed for guargum/MWCNT composites wherein, the peaks of MWCNT disappear. This is due to enhanced dispersion of MWCNT in guar gum as similarly reported by Roman *et.al.,* [**19**]. Exfoliation of nanoclay leads to increased interactions via Van der Waals forces and hydrogen bonding leading to enhanced dye removal as similarly observed by other researchers [**20,21**]. Similar trend has been observed in MWCNT composites for the removal of dyes due to increased interactions between the nanocomposites and the dyes [**22,23**].

Swelling behavior of nanocomposites in acidic, neutral and alkaline buffer solutions

Fig. 3(a-c) showed the swelling behaviour of GG-g-AA with time in acidic (pH 4), basic (pH 9) and neutral medium (pH 7). All the nanocomposites showed similar swelling behaviour with time in different buffer solutions. From **Fig. 3(a-c)** it can be seen that the nanocomposites depicted high rate of swelling till 70 minutes, after that the equilibrium is reached.

All the nanocomposites showed similar swelling pattern, highest in neutral medium and lowest in acidic medium. GG-g-AA consists of hydrophilic -COOH and -OH groups. These groups ionize as the pH of the medium increases beyond acidic range. This phenomenon exerts electrostatic repulsion leading to the expansion of polymer chains. As a result, diffusion of water molecules towards the hydrogel network takes place which attributed towards higher swelling property [**24**]. Addition of nanomaterials (both nanoclay and MWCNT) reduces the equlibrium swelling values in all the buffer solutions. This might happen due to the aggregation of nanomaterials in the hydrogel network. This in turn decreases elasticity of the polymer chain leading to lowering of swelling rates [**25**].

Swelling kinetics

Linearized pseudo-second order swelling kinetic model has been used to assess the swelling kinetics of GG-g-AA nanocomposites in acidic, neutral and alkaline medium. Linearized pseudo-second order swelling kinetic model can be represented as Equation 1 [**26**].

$$\frac{t}{Ei} = \frac{1}{ki} + \left(\frac{1}{Ei}\right)t \qquad (1)$$

where, E_t is the swelling (g/g) at a given time t (minutes), E_i is the theoretical equilibrium swelling (g/g), K_i is the initial swelling rate constant (g/g/min).

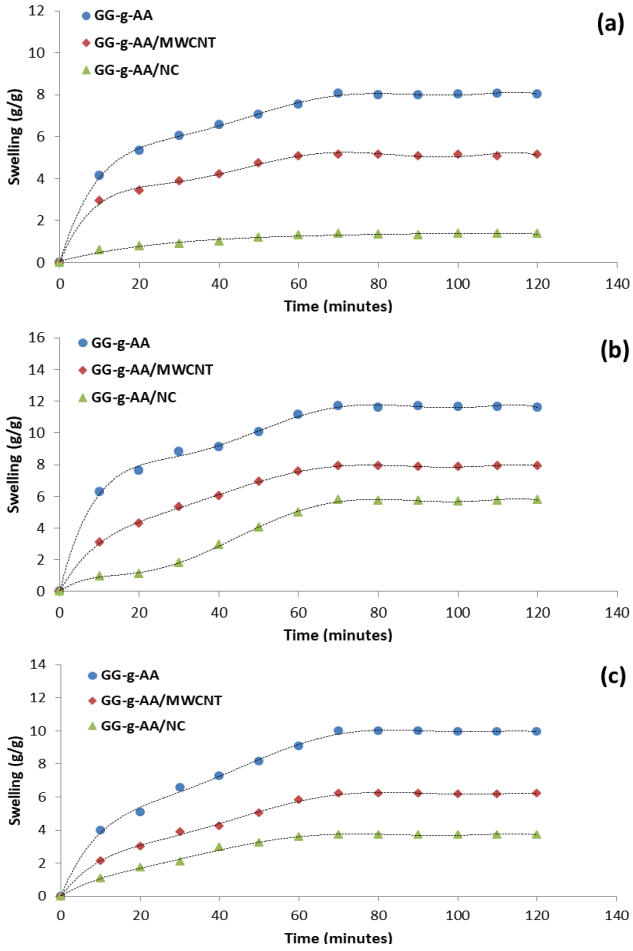

Fig. 3. Swelling characteristics of nanocomposites in (a) acidic (pH 4) medium, (b) neutral (pH 7) medium and (c) basic (pH 9) medium.

Table 1. Equilibrium swelling values and linearized pseudo-second order kinetic parameter of nanocomposites in various buffer medium.

Sample	Buffer Solution pH 4				Buffer Solution pH 9			
	E_S	E_i	K_i	<R^2>	E_S	E_i	K_i	<R^2>
GG-g-AA	8.08	9.09	0.873	0.99	9.98	10.37	0.513	0.99
GG-g-AA/N	1.38	1.64	0.082	0.99	3.72	4.14	0.157	0.97
GG-g-AA/MWCN	5.17	5.71	0.514	0.99	6.22	7.03	0.276	0.98

Sample	Buffer Solution pH 7			
	E_S	E_i	K_i	<R^2>
GG-g-AA	11.69	12.21	0.984	0.99
GG-g-AA/NC	5.78	6.05	0.136	0.99
GG-g-AA/MWCNT	7.92	8.32	0.458	0.99

Experimental results for t/Es versus t plots showed a straight line with linear correlation coefficient <R2> value greater than 0.96. This indicates the aptness of this model for assessment of kinetic swelling behavior of GG-g-AA nanocomposites. By using equation 1, swelling kinetic parameters like swelling rate constant (K_i) and theoretical equilibrium adsorption (E_i) were calculated from the slope and intercept of the linear lines shown in **Fig. 4(a-c)**. These values are listed in **Table 1**. It can be observed that experimental results (E_S) matched closely with the theoretical results (E_i) from linearized pseudo-second order kinetic model.

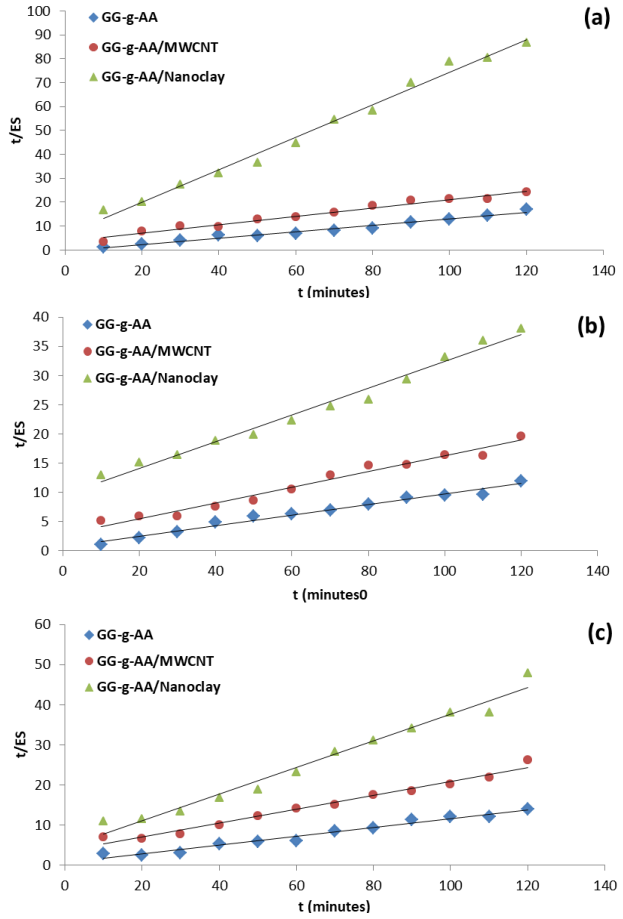

Fig. 4. Linearized form of pseudo-second order kinetic model for nanocomposites in (a) acidic (pH 4) medium, (b) neutral (pH 7) medium and (c) basic (pH 9) medium.

Adsorption isotherm models and dye removal studies

The linearized form of Langmuir and Freundlich isotherms are shown in **Fig. 6 – Fig. 9**. Langumuir adsorption isotherm assumes that each site is homogeneous and can hold a single adsorbate molecule. Freundlich isotherm on the other hand assumes heterogeneous adsorption wherein the stronger binding sites are first occupied.

The grafted guar gum (without nanoparticles) shows an increase in the percentage of dye removal for an adsorbent dosage of 100 mg and 150 mg. However, for higher i.e., 200 mg, the dye removal efficiency reduced (**Fig. 5**). The increase in dye removal up to 150 mg of adsorbent is due to increased surface area and adsorption sites. At 200 mg, the reduction is mainly due to excess adsorbent available while adsorbate availability is less. This in turn causes a flux gradient between the grafted adsorbent and the dye [**27,28**]. Further, for 100 mg and 150 mg adsorbent dose, an increase in initial dye concentration led to enhanced dye removal. However, this trend is not observed for 200 mg adsorbent dosage. At higher initial dye concentration, the active adsorption sites have access to large number of dye molecules, which led to increased dye adsorption for lower adsorbent dosages [**29**]. A similar observation wherein, dye removal increases with initial dye concentration and lowered adsorbent dosage has also been observed by Nsami *et.al.*, [**30**]. However, at higher adsorbent dosage (200mg), increased initial dye concentration shows lower dye efficiency (as compared to that at 100 mg and 150 mg) owing to increased competition between the active adsorbent sites and available dye molecules. The results obtained were fitted for both Langmuir and Freundlich adsorption isotherms (**Fig. 6**). The $<R^2>$ values indicate that the Langmuir isotherm showed a better agreement than the Freundlich model. Hence, this suggests that monolayer homogeneous type of adsorption is the dominant mechanism (as per Langmuir isotherm model) of dye adsorption. Further, at lower adsorbent dosage of 100 mg the $<R^2>$ values indicate that both Freundlich isotherm and Langmuir models fitted well indicating that both homogeneous and multilayer adsorption took place. Further, the KL value i.e., the adsorption equilibrium constant (from Langmuir model) did not vary considerably with the adsorbent dosage. The q_{max} value obtained showed increased with the adsorbent dosage as shown in **Table 2**. The percentage dye removal improved as the initial concentration increased as the driving force was enhanced. However, an adsorbent dosage of 150 mg showed the optimal dye removal as compared to 100 mg and 200 mg adsorbent (**Fig. 5**). At 200 mg adsorbent dosage, the dye removal efficiency reduced suggesting that the adsorption sites are saturated [**31**].

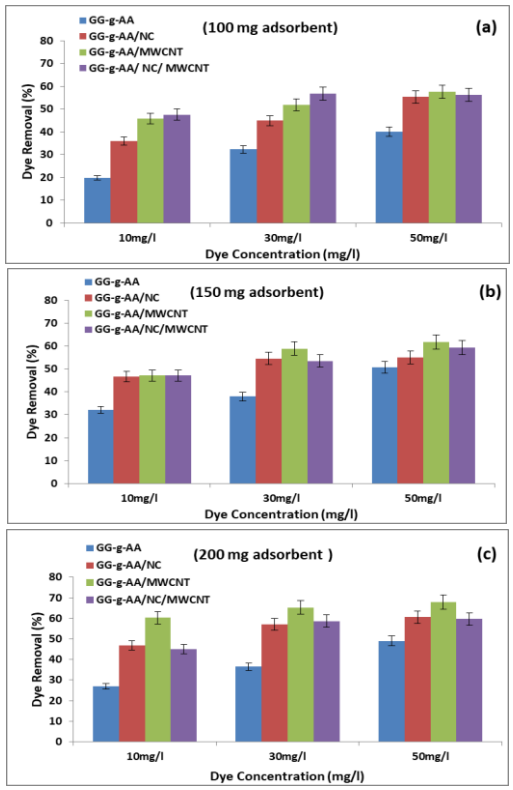

Fig. 5. Percentage of Crystal Violet dye removal efficiency of nanocomposites with varying initial dye concentration and varying adsorbent dosage.

Table 2. Langmuir and Freundlich isotherm parameters for Crystal Violet dye adsorption onto GG-g-AA composites (100, 150 & 200 mg adsorbent dosage).

Sample (GG-g-AA)	Langmuir Isotherm			Freundlich Isotherm		
Adsorbent Dosage	q_m (mg/g)	K_L (L/mg)	$<R^2>$	1/nF	K_F ($mg^{1-1/n} L^{1/n} g^{-1}$)	$<R^2>$
100mg	98.04	0.021	0.99	0.573	1.92	0.99
150mg	103.09	0.028	0.99	0.581	1.19	0.975
200mg	117.65	0.031	0.99	0.702	1.98	0.952

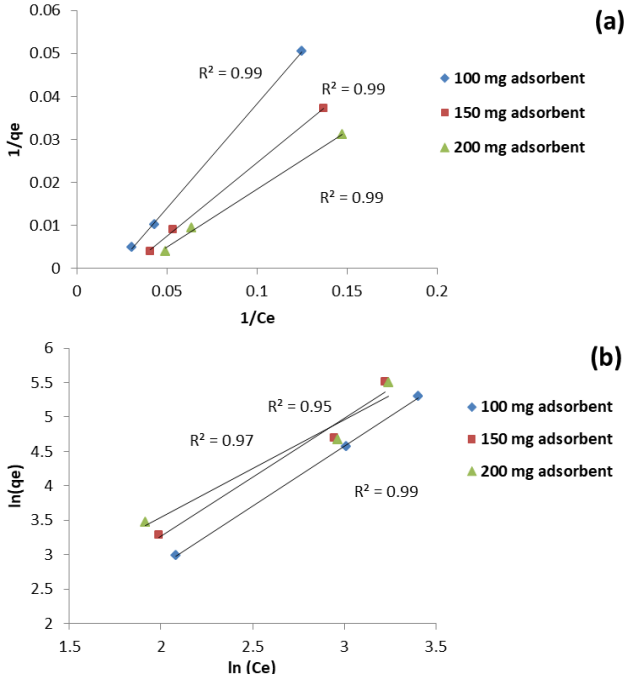

Fig. 6. (a) Langmuir isotherms; (b) Freundlich isotherms for crystal violet dye adsorption by GG-g-AA.

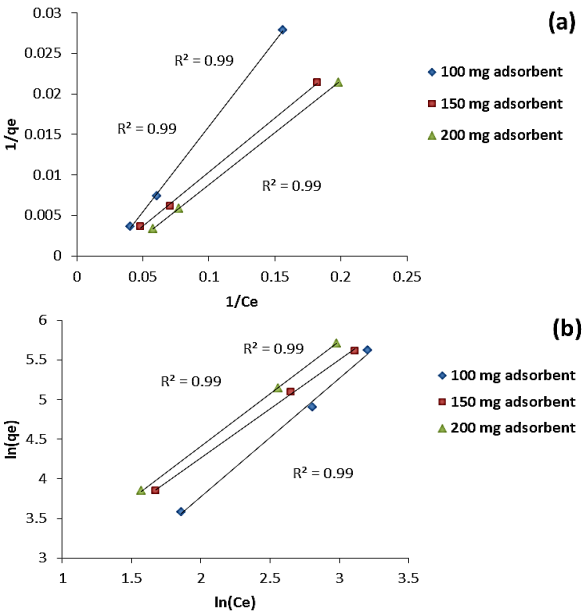

Fig. 7. (a) Langmuir isotherms; (b) Freundlich isotherms for crystal violet dye adsorption by GG-g-AA/Nanoclay.

Addition of nanoclay to grafted guar gum increases the adsorption capacity (Fig. 5) as compared to composites without nanoclay. As the adsorbent dosage increases, the percentage dye removal also increases. This trend can also be seen with increase in initial dye concentration. The observed results were fitted with the adsorption models. It can be seen that obtained data fitted both Langmuir and Freundlich models (**Fig. 7**). This suggests that the adsorption mechanism was a mixture of both homogeneous as well as multi-layered heterogeneous in nature [**32**]. The $<R^2>$ values were all above 0.99 (**Table 3**) for both the isotherms and similar results have also been reported by Chauhan *et. al.*, [**33**]. The inclusion of nanoclay further increased the surface which facilitated enhanced adsorption. Similar effect of increased adsorption has been observed by Mahdavinia *et.al.*, by inclusion of montmorillonite to carrageenan [**34**]. Further, XRD profiles also indicated exfoliation of nanoclay which also suggests good dispersion which in turn helps increase the dye removal efficiency. Also, lower nanoclay content (in this case, 0.5%) shows favourable dye adsorption capabilities as has been similarly observed by Seddiki *et.al.*, [**35**].

Table 3. Langmuir and Freundlich isotherm parameters for Crystal Violet dye adsorption onto GG-g-AA/Nanoclay nanocomposites (100, 150 & 200 mg adsorbent dosage).

Sample (GG-g-AA/ Nanoclay)	Langmuir Isotherm			Freundlich Isotherm		
Adsorbent Dosage	q_m (mg/g)	K_L (L/mg)	$<R^2>$	1/nF	K_F ($mg^{1-1/n} L^{1/n} g^{-1}$)	$<R^2>$
100mg	196.07	0.024	0.99	0.669	2.19	0.99
150mg	322.58	0.023	0.99	0.808	5.97	0.99
200mg	243.89	0.031	0.99	0.757	5.88	0.99

The effect of adding modified MWCNT to grafted guar gum is showed in Fig. 5. It can be seen as the nanocomposite adsorbent dosage increases, the percentage dye removal increased. Further, the dye removal capability is higher than that of neat, grafted guar gum (i.e., without nanoparticles) or nanoclay loaded grafted guar gum. The performance of MWCNT than either grafted guar gum or nanoclay loaded grafted gum may be attributed to higher affinity to crystal violet towards the nanotubes [**36**]. The hydrophilicity of MWCNT is enhanced by acid modification. This also facilitates adsorption of dye [**37**]. Further, as the initial dye concentration increases, dye removal efficiency increased for each adsorbent dosage. A similar observation has been made by Idan *et.al.*, [**38**]. It was argued that as the initial dye concentration increases interaction between the dye and adsorbent increases. This leads to increased driving force for adsorption owing to reduced mass transfer resistance. Langmuir and Freundlich isotherm models have been fitted for these composites (**Fig. 8**). In this case too, the observed results agree with both the models. In both cases $<R^2>$ values is greater than 0.99 (**Table 4**). Hence adsorption mechanism is both homogeneous and multi-layered in nature [**39**]. The increased adsorption with the adsorbent dosage is due to

increased surface area and hence availability of more adsorption sites [**40**].

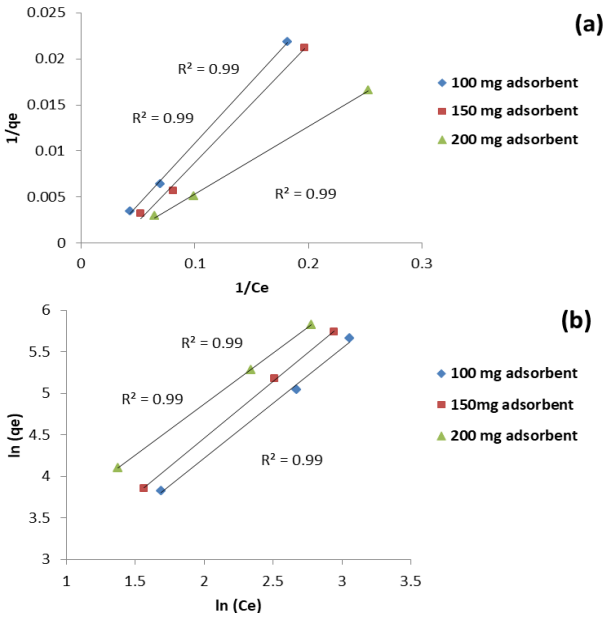

Fig. 8. (a) Langmuir isotherms; (b) Freundlich isotherms for crystal violet dye adsorption by GG-g-AA/MWCNT.

Table 4. Langmuir and Freundlich isotherm parameters for Crystal Violet dye adsorption onto GG-g-AA/MWCNT nanocomposites (100, 150 & 200 mg adsorbent dosage).

Sample (GG-g-AA/MWCNT)	Langmuir Isotherm			Freundlich Isotherm		
Adsorbent Dosage	**q_m (mg/g)**	**K_L (L/mg)**	**$<R^2>$**	**$1/n_F$**	**K_F ($mg^{1-1/n} L^{1/n} g^{-1}$)**	**$<R^2>$**
100mg	384.61	0.019	0.99	0.752	4.77	0.99
150mg	250	0.031	0.99	0.731	5.57	0.99
200mg	476.19	0.028	0.99	0.810	10.8	0.99

Fig. 5 shows the effect of including both nanoclay as well as carbon nanotubes. It can be seen that as the initial dye concentration increases, the dye removal percentage also increased. However, addition of both nanosized particles together did not increase the dye removal capability. In facts, it can be seen that there is a slight reduction in percentage dye removal when both types of nanoparticles are used. In this case obtained data fitted both Langmuir and Freundlich isotherm models (**Fig. 9**). The $<R^2>$ values were higher than 0.98 (**Table 5**).

Table 5. Langmuir and Freundlich isotherm parameters for Crystal Violet dye adsorption onto GG-g-AA/ Nanoclay + MWCNT nanocomposites (100, 150 & 200 mg adsorbent dosage).

Sample (GG-g-AA/Nanoclay + MWCNT)	Langmuir Isotherm			Freundlich Isotherm		
Adsorbent Dosage	**q_m (mg/g)**	**K_L (L/mg)**	**$<R^2>$**	**$1/n_F$**	**K_F ($mg^{1-1/n} L^{1/n} g^{-1}$)**	**$<R^2>$**
100mg	370.37	0.017	0.99	0.829	5.14	0.99
150mg	333.33	0.023	0.99	0.712	4.21	0.99
200mg	212.76	0.043	0.99	0.601	3.08	0.98

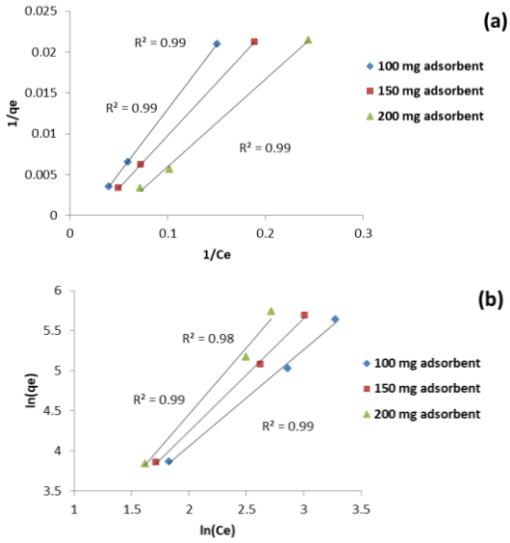

Fig. 9. (a) Langmuir isotherms; (b) Freundlich isotherms for crystal violet dye adsorption by GG-g-AA/ Nanoclay +MWCNT.

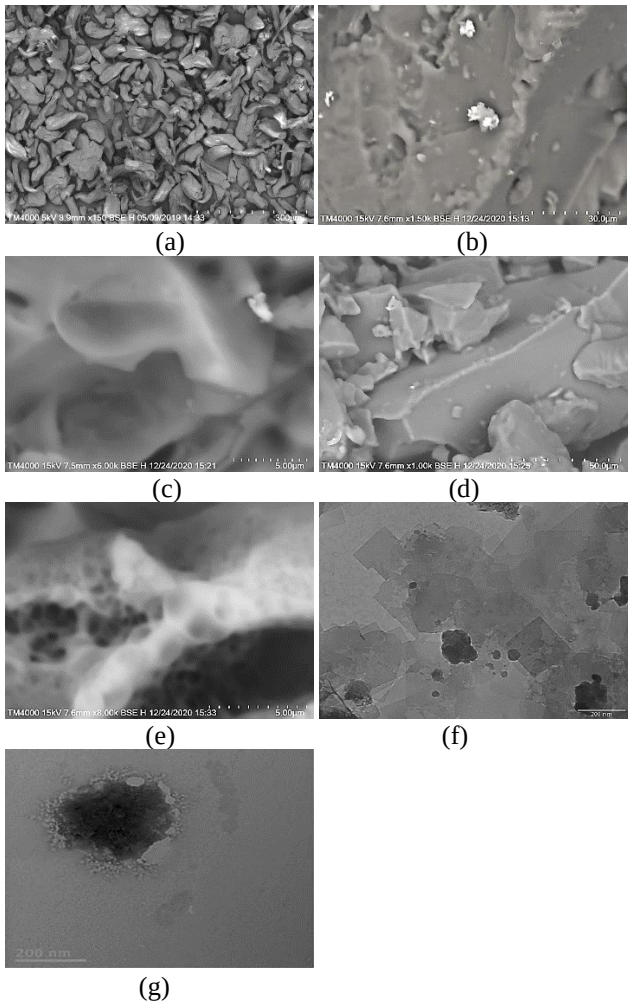

Fig. 10. (a) SEM micrograph of pure guar gum. (b) & (c) SEM micrograph of GG-g-AA/Nanoclay composite. (d) & (e) SEM micrograph of GG-g-AA/MWCNT composite. (f) TEM micrograph of GG-g-AA/Nanoclay composite. (g) TEM micrograph of GG-g-AA/MWCNT composite.

Morphology

The SEM micrographs of guar gum grafted acrylic acid loaded with nanoclay and MWCNT is shown in **Figs. 10 (a-g)**. Neat guar gum (**Fig. 10(a)**) shows a granular structure. However, grafted guar gum with nanoclay shows mixed morphological features with lamellar structure intermixed with agglomerated particles. The morphological part is partly continuous owing to network formation contributed by both inter-chain bonding of carboxylic groups [**41**]. This also suggests enhanced interactions between guar gum and acrylic acid [**42**]. Such roughness leads to increased surface area, thereby leading to enhanced adsorption as compared to neat grafted guar gum [**Figs. 10(b)** & **10(c)**]. This is also reflected higher adsorption capacity of the nanoclay loaded composite as compared to neat guar gum. SEM micrographs of grafted guar gum/ MWCNT composites is shown in **Fig. 10(d)** and **Fig. 10(e)**. Grafting and inclusion of MWCNT shows a change in morphology i.e., from granular to smooth lamellar continuous surface [**43**]. The SEM micrograph at higher magnification shows bulged surface indicating wrapping of MWCNT with grafted guar gum. Hence, such rough surface morphology leads to increased surface area and adsorption sites facilitating enhanced dye removal capabilities [**44,45**]. The TEM micrographs show dispersed nanoclay particles with regions of agglomeration (**Fig. 10(f)**). While the MWCNT dispersion can be seen throughout with regions of clustering (**Fig. 10 (g)**).

Conclusion

Guar gum grafted acrylic acid nanocomposites have been synthesized using NC and MWCNT either alone or in combinations. The grafting reaction has been carried out following microwave assisted method. All the nanocomposites showed highest swelling in neutral medium and lowest in acidic medium. Swelling kinetics of all the nanocomposites followed pseudo second order kinetic model with $<R^2>$ value more than 0.98. Among the synthesized nanocomposites the one with MWCNT showed highest amount of crystal violet dye removal efficiency compared to the other nanocomposites. XRD studies showed enhanced dispersion and exfoliation of nanomaterials in the composite. Morphological studies showed rough surface morphology of the nanocomposites. Thus, the synthesized nanocomposites showed potential for removal of toxic crystal violet dye from aqueous solutions.

Conflicts of interest
There are no conflicts to declare.

Keywords
Guar gum, adsorption isotherm, nanoclay, MWCNT, dye removal.

References

1. Sharma, G.; Sharma, S.; Kumar, A.; Al-Muhtaseb, A.H.; Naushad, M.; Ghfar, A.A.; Mola, G.T.; Stadler, F.J.; *Carbohyd. Polym*., **2018**, *199*, 534-545.
2. Verma, A.K.; Dash, R.R.; Bhunia, P.; *J. Environ. Manage.;* **2012**, *93*, 154.
3. Mittal, H.; Ray, S.S.; Okamoto, M.; *Macromol. Mater. Eng*., **2016**, *301*, 496.
4. Ahmad, R.; Mirza, A.; *J. Mol. Liq*., **2018**, *249*, 805-814.
5. Duan, M.; Ma, J.; Fang, S.; *Carbohyd. Polym.*, **2019**, *211*, 308.
6. Vanaamudan, A.; Sadhu, M.; Pamidimukkala, P.; *J. Mol. Liq.*, **2018**, *271*, 202.
7. Patra, A.S.; Ghorai, S.; Ghosh, S.; Mondal, B.; *J. Hazard. Mater.*, **2016**, *301*, 127.
8. Sharma, G.; Kumar, A.; Sharma, S.; Al-Muhtaseb, A.H.; Naushad, M.; Ghfar, A.A.; Ahamad, T.; Stadlar, F.J.; *Sep. Purif. Technol.*, **2019**, *211*, 895.
9. Sharma, R.; Kaith, B.S.; Kalia, S.; Pathania, D.; Kumar, A.; Sharma, N.; Street, R.M.; Schauer, C.; *J. Environ. Manage*., **2015**, *162*, 37.
10. Sahoo, J.K.; Kumar, A.; Rath, J.; Mohanty, T.; Dash, P.; Sahoo, H.; *Desalin. Water Treat.*, **2017**, *95*, 342.
11. Makhado, E.; Pandey, S.; Nomngongo, P.; Ramontja, J.; Xanthan gum-cl-poly (acrylic acid) / Reduced Graphene Oxide Hydrogel Nanocomposite as Adsorbent for Dye Removal. 9th Int'l Conference on Advances in Science, Engineering, Technology & Waste Management, **2017**, *1*, 159-164.
12. Dassanayake, R.S.; Rajakaruna, E.; Abidi, N.; *J. Nanomater*., **2019**, 1-11.
13. Saxena, R.; Sharma, S.; *Int. J. Sci. Eng. Res.*, **2016**, *7*, 675.
14. Pakdel, P.M.; Peighambardoust, S.J.; *J. Environ. Manage.*, **2018**, *217*, 123.
15. Shruthi, S.B.; Bhat, C.; Bhaskar, S.P.; Preethi, G.; Sailaja, R.R.N.; *Green. Sustainable. Chem.*, **2016**, *6*, 11.
16. Sharma, Reena; Kalia, Susheel; Kaith, Balbir. S.; Srivastava, Manoj. K.; *Int. J. Plast. Technol.*, **2016**, *20*, 294.
17. Salam, M.A.; Burk, R.; *Arabian. J. Chem.*, **2012**, *10*, 921.
18. Yoonessi, M.; Toghiani, H.; Kingery, W.L.; Pittman Jr, C.U.; Preparation, Characterization, and Properties of Exfoliated/ Delaminated Organically Modified Clay/Dicyclopentadiene Resin Nanocomposites. Macromolecules, **2004**, *37*, 2511.
19. Roman, C.; Morales, M.G.; Gupta, J.; McNally, T.; On the phase affinity of multi-walled carbon nanotubes in PMMA: LDPE immiscible polymer blends. Polymer, **2017**, *118*, 1-11.
20. Atta, A.M.; Al-Lohedan, H.A.; ALOthman, Z.A.; Abdel-Khalek, A.A.; Tawfeek, A.M.; *J. Ind. Eng. Chem.*, **2015**, *31*, 374.
21. Salam, M.A.; Kosa, S.A.; Al-Beladi, A.A.; *J. Mol. Liq*., **2017**, *241*, 469.
22. Rajabi, M.; Mahanpoor, K.; Moradi, O.; *RSC. Adv*., **2017**, 7, 47083.
23. Pan, B.; Xing, B.; *Environ. Sci. Technol.*, **2009**, *42*, 9005.
24. Poorna Chandrika, K.S.V.; Singh, A.; Sarkar, D.J.; Rathore, A.; Kumar, A.; *J. Appl. Polym. Sci.*, **2014**, *1*, 1.
25. Peng, N.; Hu, D.; Zeng, J.; Li, Y.; liang, L.; Chang, C.; *ACS. Sustain. Chem. Eng*., **2016**, *4*, 7217.
26. Ho, Y.S.; McKay, G.; *Process. Biochem*., **1999**, *34*, 451.
27. Nandi, B.K.; Goswami, A.; Das, A.K.; Mondal, B.; Purkait, M.K.; *Sep. Sci. Technol*., **2008**, *43*, 1382.
28. Niran, O.B.; Olawale, S.A.; Ushie, U.J.; *Asian. J. Appl. Chem. Res.* **2018**, *1*, 1.
29. Gorzin, F.; Abadi, M.B.R.; *Adsorp. Sci. Technol*., **2018**, *36*, 149.
30. Nsami, J.N.; Mbadcam, J.K.; *J. Chem.*, **2013**, 1.
31. Desta, M.B.; *J. Thermodyn*., **2013**, 1-6.
32. Khan, T.A.; Nazir, M.; Ali, I.; Kumar, A.; *Arab. J. Chem.*, **2013**, *10*, 2388.
33. Chauhan, K.; Chauhan, G.S.; Ahn, J.H.; *Bioresour. Technol*., **2009**, *100*, 3599.
34. Mahdavinia, G.R.; Zhalebaghy, R.; *J. Mater. Environ. Sci.*, **2012**, *3*, 895.
35. Seddiki, N.; Aliouchi, D.; Boudhene, I.; *Rev. Roum. Chim*., **2020**, *65*, 119.
36. Hosseinzadeh, H.; *Pol. J. Chem. Technol*., **2015**, *17*, 70.
37. Ferreira, G.M.D.; Ferreira, G.M.D.; Hespanhol, M.C.; Rezende, J.P.; Pires, A.C.S.; Gurgel, L.V.A.; Silva, L.H.M.; *Colloids. Surf. A*., **2017**, *529*, 531.

38. Idan, I.J.; Abdullah, L.C.; Choong, T.S.; Jamil, S.N.A.B.; *Adsorpt. Sci.Technol*., **2017**, 1-19.
39. Kumar, P.S. Sivaprakash, S.; Jayakumar, N.; *Int. J. Mater. Sci.*, **2017**, *1*, 107.
40. Mohammed, M.I.; Abdul Razak, A.A.; Al-Timimi, D.A.H.; *Adv. Mater. Sci. Eng.*, **2014**, 1-10.
41. Dharela, R.; Raj, L.; Chauhan, G.S.; *J. Appl. Polym. Sci.*, **2012**, *126*, 259.
42. Huang, Y.; Lu, J.; Xiao, C.; *Polym. Degrad. Stab.*, **2007**, *92*, 1072.
43. Dong, L.; Zhu, J.; Xiao, W.; *Adv. Mater. Res.*, **2012**, 535.
44. Zhao, D.; Zhang, W.; Chen, C.; Wang, X.; *Proc. Env. Sci.*, **2013**, *18*, 890.
45. Saxena, R.; Sharma, S.; *Int. J. Sci. Eng. Res*., **2016**, *7*, 675.